http://dx.doi.org/10.21622/ACE.2022.02.2.068

A Multi-band MIMO Antenna System with Coupled-fed Modified Rectangular Patch Elements for 5G Systems

Marwa H. Sharaf *, Amira I. Zaki, Radwa K. Hamad and Mohamed M. M. Omar

Electronics and Communications Department, College of Engineering and Technology, Arab Academy for Science, Technology & Maritime Transport, Alexandria 21937, Egypt

Email: {00000, amzak10@aast.edu, radwa_hamad@aast.edu, abuahmad.omar@aast.edu}

Received on, 18 September 2022 - Accepted on, 02 November 2022 - Published on, 22 November 2022

ABSTRACT

A four-port multiple input multiple output (MIMO) antenna system constructed of four compact dual-band (38/60 GHz) microstrip patch antennas is proposed for 5G mobile applications. Each individual element is optimized to achieve the desired performance of the overall MIMO system. Numerical and experimental investigations are achieved to assess the performance of both the single-element antenna and the four-port MIMO antenna system. It is shown that the simulation results agree with the experimental measurements, and both show good performance of the proposed MIMO antenna system. The bandwidths achieved around 38 GHz and 60 GHz are about 2 GHz and 3.2 GHz, respectively. The performance of the MIMO antenna system including the return loss at each antenna port and the coupling coefficients between the different ports are investigated. The radiation patterns produced when each port is excited alone are shown to be suitable for spatial diversity scheme. They have a high radiation efficiency exhibited by a balloon-like shaped radiation pattern for both the upper and lower frequency bands. It is shown that the envelope correlation coefficient (ECC) and the diversity gain (DG) are suitable for performance for the targeted 5G bands.

Index Terms: MIMO, dual-band, 5G mobile, mobile terminal, microstrip patch antenna, antenna design, diversity.

1. INTRODUCTION

The need for endless users joining the network with high rates of information being sent and received has been the driving force behind the boom of the auspicious Fifth-Generation (5G) technology [1]. The data rates have massively exploded to reach 100 times nowadays and as expected, 1000 times by 2030 [2]. Multi-input-multi-output (MIMO) techniques play an important role in increasing the wireless channel capacity by deploying multiple antennas at the transmitter and the receiver without the need for additional power or spectrum [3-5]. Diversity schemes are considered to be a key component to combat fading and enhance the wireless link reliability by sending the same signals by uncorrelated antennas.

The abandoned Millimeter-wave spectrum (30-300 GHz) wave is anticipated to be a dominant factor due to its multi-Gigabit/s transmission rate possessing the wide available bandwidth to fulfil the demands of the proliferation of 5G applications which require high quality and low latency transmission [6-9]. The Federal Communications Commission (FCC) has allocated the bands of 59-64 GHz for high

http://dx.doi.org/10.21622/ACE.2022.02.2.068

speed wireless communications and short range as an unlicensed band [10]. The International Telecommunications Union (ITU) has allocated the frequency bands which are centered at 28, 38, 60 and 73 GHz for 5G mobile communications [11]. Mobile phones are restricted by a very limited space which highlights a difficult challenge to integrate several antenna elements with high isolation which is a vital necessity for a MIMO antenna system with a good performance [12-15]. The proposed dual-band MIMO antenna in the present work utilizes the 38-GHz frequency band (potential candidate for next generation communication) and the 60-GHz frequency in a single compact antenna to be properly allocated to achieve excellent isolations between all elements.

Recently, many designs for mobile handset antennas for 5G applications are provided. In the work of [16], the MIMO antenna system operate in the 28 and 38 GHz bands by two ports which are realized by two antenna arrays. The work of [17] is concerned with the dual band (28/38 GHz) which gives the duality by the main radiator being etched by an inverted U-shaped slot. The work of [18] adopts three stacked patches to work in the dual band (28/38 GHz). In [19], a MIMO antenna system is designed to serve the fourth generation (4G) with a bandwidth of 2 GHz and 5G bands of (28, 37 and 39 GHz) on a single antenna. Each element in the system consists of a slot-based antenna and is fed by two microstrip feeders. The work of [20] investigates a 60 GHz array of antennas which are composed of feedlines, ground and parasitic elements. As specified in [21], the isolation between the meander-line dual-band antennas is achieved by a split electromagnetic band gap structure where the antenna is coupled to a parasitic patch to achieve the duality of bands. The splits applied are to decouple at the first resonant mode and utilize the Electromagnetic Band Gap (EBG) to decouple at the second resonant mode. The work of [22] presents a compact antenna design to work as a single element antenna or can be integrated to a MIMO antenna system working in the dual frequency band of (38/60 GHz) for 5G mobile communications systems.

The present work proposes a four-port MIMO antenna system for 5G mobile phones composed of modified rectangular patch antenna shown in [22]. The proposed modified rectangular patch antenna is composed of two patches; the primary patch is directly fed through a microstrip line with inset feed whereas the secondary patch is indirectly fed by coupling to the primary patch. A four-port MIMO antenna system is constructed of four elements of the proposed modified microstrip patch antenna. The separations between the four antennas lead to the spatial diversity required for the targeted 5G applications allowing high performance at high data rates. The MIMO antenna system performance including the return loss at each antenna port and the coupling coefficients between the different ports is investigated and shown to be suitable for 5G mobile communications. The radiation patterns produced when each port is excited alone are shown to be suitable for an efficient diversity scheme. The performance measures such as the envelope correlation coefficient (ECC) and diversity gain (DG) are evaluated showing excellent performance of the proposed MIMO antenna system.

The remaining part of the proposed paper is organized as follows. Section 2 proposes a four-port MIMO antenna system that employs antenna diversity for enhancement of the wireless channel performance. Section 3 presents the simulation results concerned with the proposed modified patch and the MIMO antenna system performance with detailed discussions. Section 4 is dedicated to describe the antenna fabrication and the experimental measurements. Section 5 includes comparisons between the results of the present work and those presented in other published work. Finally, Section 6 is devoted to the most important conclusions of the present work.

http://dx.doi.org/10.21622/ACE.2022.02.2.068

2. THE PROPOSED FOUR-PORT MIMO ANTENNA SYSTEM FOR USER EQUIPMENT

To construct an optimized compact-size dual-band MIMO antenna system with low loss and minimum power consumption, it is proposed to use a dual-band small-size radiating element. The dimensions of the single element are given in Figure 1(a) where the dimensions are inspired by the design of [22]. It is designed to radiate in the dual frequency bands centered at 38 and 60 GHz. This antenna can be viewed as composed of two patches; the first patch is fed through a direct microstrip line with an inset feed, while the second is fed through capacitive (edge) coupling with the first patch.

The dimensions of the first patch are designed so that the first patch operates in its first-order mode at 38 GHz while the combined structure of the first and second patches is designed to have its first-order mode radiating at 60 GHz. At 38 GHz the radiation pattern is produced by the well-known first-order mode of the first patch which is omnidirectional in the azimuth plane (x-y) and has a balloon-like shape in the (elevation) E- and H-planes. The second patch has no contribution to the radiation at 38 GHz because of its small dimensions and the gap separation between both patches.

On the other hand, the cuts made in the first patch, specifically at the corners on both sides of the microstrip line, help to diminish the slot fields and surface currents near these regions thus preventing the formation of higher-order modes in the cavity below the combined-patch structure. Consequently, the radiation pattern at 60 GHz has a shape which is similar (to some extent) to that radiated by a rectangular patch operating at its first-order resonance.

TABLE 1. Dimensions of Design "A".

Dimension	Value (mm)
LP_1	2.05
LP_2	1.2
WP_1	2.6
WP_2	1.42
GP	0.6
L_{ins}	0.739
W_{ins}	0.11

To construct a four-port MIMO antenna system for operation at 38/60 GHz, four elements of the dual-band microstrip patch antenna with the dimensions shown in Figure 1(a) are arranged as shown in Figure 1(b). The separations between the four antennas are set so as to achieve the spatial diversity required for the target 5G applications. Such a MIMO antenna system allows high data rates for mobile communications with high performance. Let the design with the dimensions presented in Figure 2 be named design "A" with the dimensions presented in Table 1. This design is compact (total dimensions 20 x 20 mm2) with short feeding lines

http://dx.doi.org/10.21622/ACE.2022.02.2.068

and reasonable separations between the four antennas. Such a MIMO antenna system can be practically suitable to be manufactured and integrated on a printed electronic board of a mobile handset as no bulky millimeter-wave connectors are required in this case. However, such an antenna system design may be inappropriate to be connected to a microwave source for the purpose of laboratory experimental investigations.

Design "B", shown in Figure 2, gives alternatives for both the single element and the four-port MIMO system designs that are more suitable for experimental investigations in millimeter-wave laboratories. The longer feedlines of this design allow experimental measurements through coaxial launch connectors. Such commercially available connectors are bulky and may affect the antenna operation if they are connected to short feedlines like those of design "A". The total area of the MIMO antenna system with design "B" is 50 x 30 mm^2, which is about four times the area of that with design "A". It should be noted that both the horizontal and vertical separations between the antenna elements in design "B" are larger than those in design "A" for the enhancement of the diversity gain.

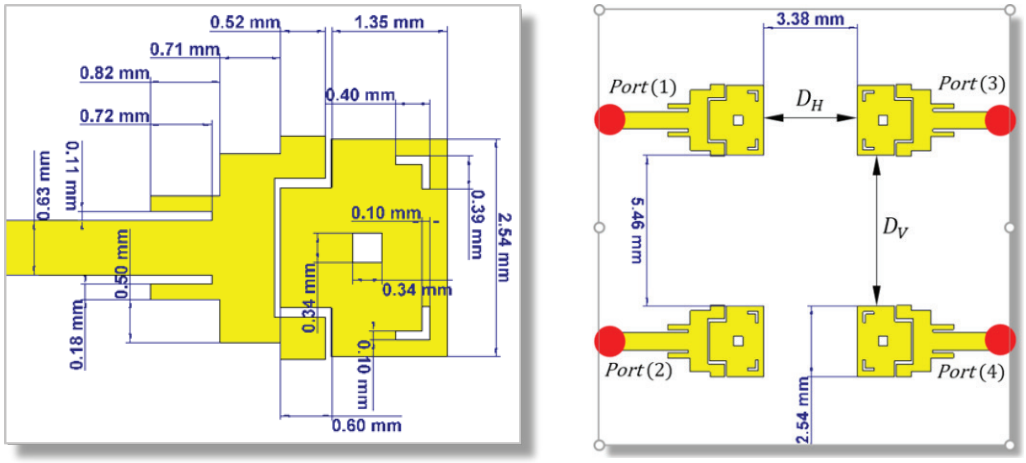

(a) (b)

Fig. 1. (a) Dual-band patch antenna, (b) Four-port MIMO antenna system (total dimensions of 20 x 20 mm^2) proposed for 5G mobile handsets (design "A").

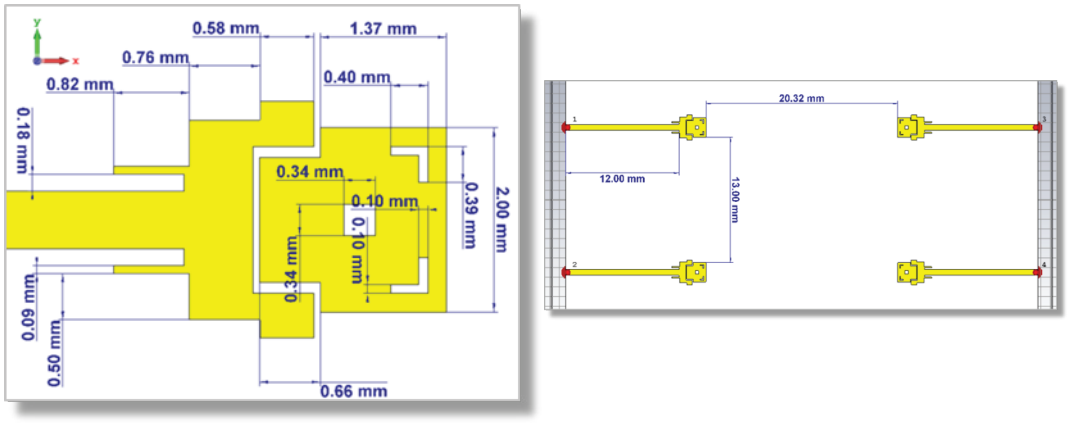

(a) (b)

Fig. 2. (a) Dual-band patch antenna, (b) Four-port dual-band MIMO antenna system (total dimensions 50 x 30 mm^2) proposed for fabrication and experimental investigation (design "B").

http://dx.doi.org/10.21622/ACE.2022.02.2.068

3. SIMULATION RESULTS AND DISCUSSION

In this section, the performance of the dual-band patch antenna and that of the four-element MIMO antenna system are investigated and the corresponding numerical results are presented and discussed. The return loss and radiation patterns of the single antenna and MIMO system are investigated. Furthermore, the results are concerned with the coupling coefficients, the radiation patterns, the diversity gain (DG) and the corresponding envelope correlation coefficient (ECC) of the four-port MIMO antenna configuration. The performance of both designs "A" and "B" for the MIMO system are investigated with experimental investigations for design "B".

3.1. Performance Assessment of the Dual-band Microstrip Patch Antenna

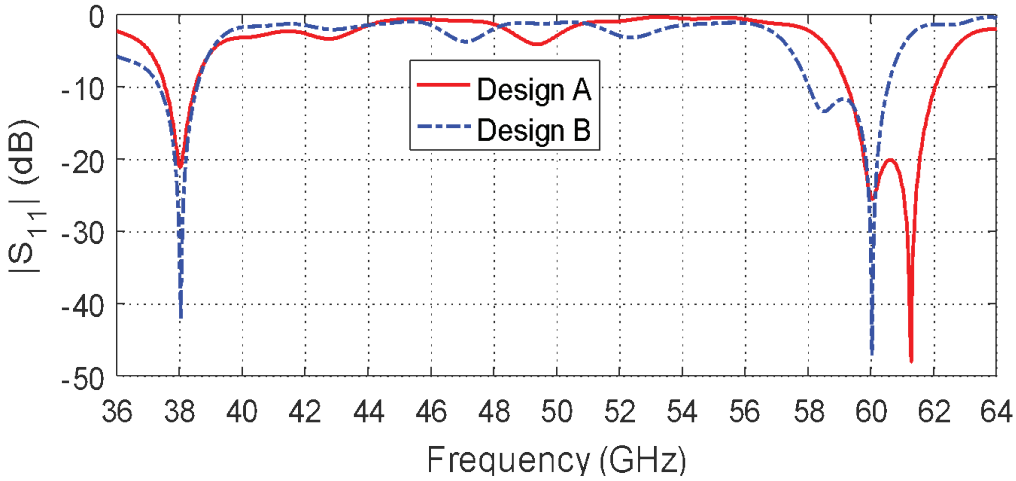

Fig. 3. Dependence of the simulated reflection coefficient, |Ss11| on a wide band of frequency for the proposed dual-patch antenna (for both designs "A" and "B").

The dependence of the simulated reflection coefficient, $|Ss_{11}|$ of the proposed dual-patch antenna is presented in Figure 3. It is shown in the figure that the antenna impedance of designs "A" and "B" are perfectly matched at the frequencies 38 and 60 GHz. Design "A" has return loss of -21 and -25 dB at 38 and 60 GHz, respectively. Design "B" is shown to have return loss of -42 and -47 at 38 and 60 GHz, respectively which outperforms design A with lower return loss at both operating bands.

The radiation patterns for the proposed dual-band antenna at 38 GHz for both design "A" and design "B" are presented in Figure 4(a) and Figure 4(b), respectively in the E-plane (ϕ =0°) and H-plane (ϕ =90°) to show that a balloon-like shape is achieved. Similarly, Figures 5(a) and 5(b) depict the balloon-like shape of the 60 GHz for designs "A" and "B". Figures 6(a) and 6(b) highlight the omnidirectional shape of the radiation patterns at 38 GHz for both designs ("A" and "B"), respectively in the azimuth planes (θ =const) in addition to the same azimuth radiation patterns obtained for 60 GHz shown in Figures 7(a) and 7(b). The maximum gain is about 6.5 dBi at 38 GHz, and is about 5.5 dBi at 60 GHz. Such radiation patterns are proper for MIMO antenna system composed of multiple units of such dual-band radiating elements.

http://dx.doi.org/10.21622/ACE.2022.02.2.068

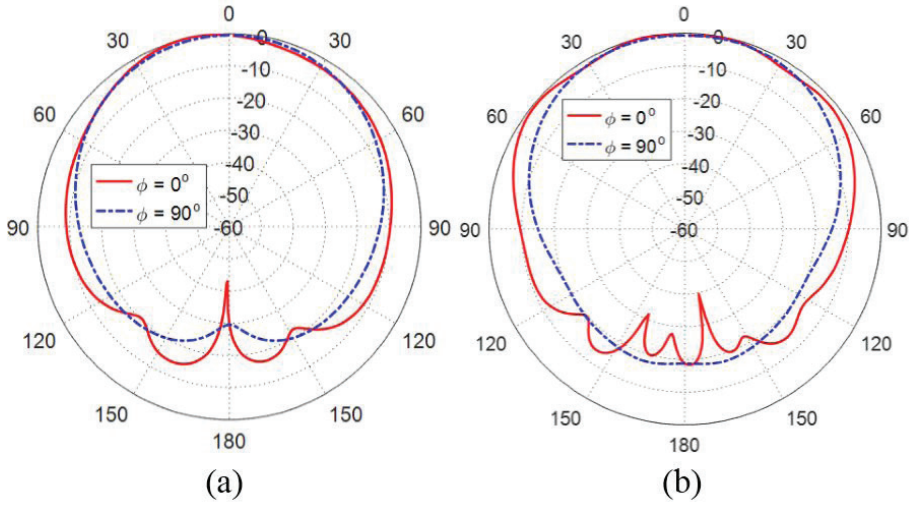

Fig. 4. Radiation patterns in the elevation planes at 38 GHz for the dual-band microstrip patch antenna, (a) design "A" and (b) design "B".

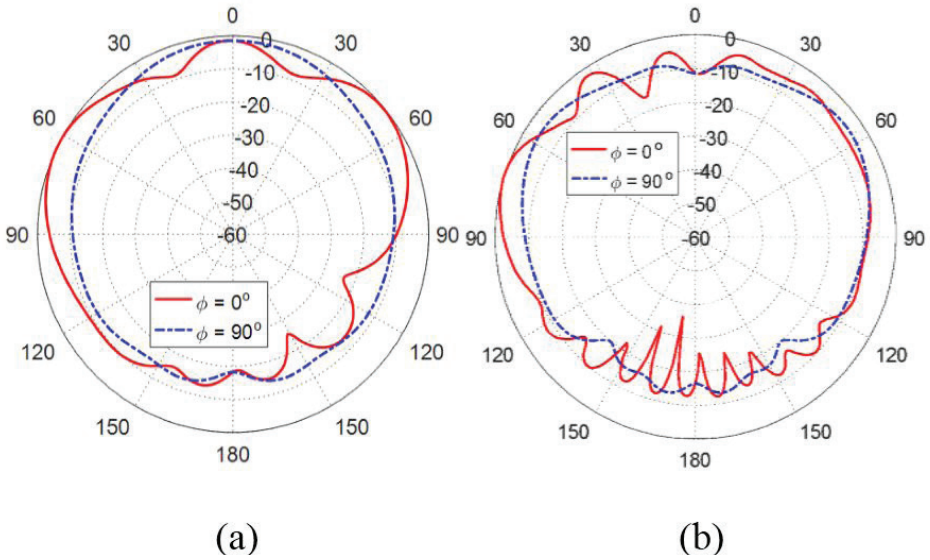

Fig. 5. Radiation patterns in the elevation planes at 60 GHz for the dual-band microstrip patch antenna, (a) design "A" and (b) design "B".

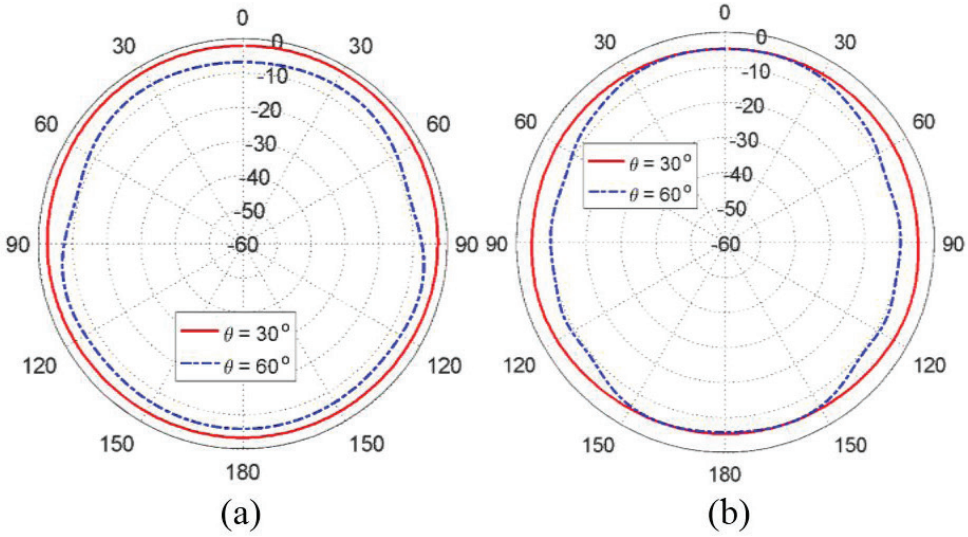

Fig. 6. Radiation patterns in the azimuth planes at 38 GHz for the dual-band microstrip patch antenna, (a) design "A" and (b) design "B".

http://dx.doi.org/10.21622/ACE.2022.02.2.068

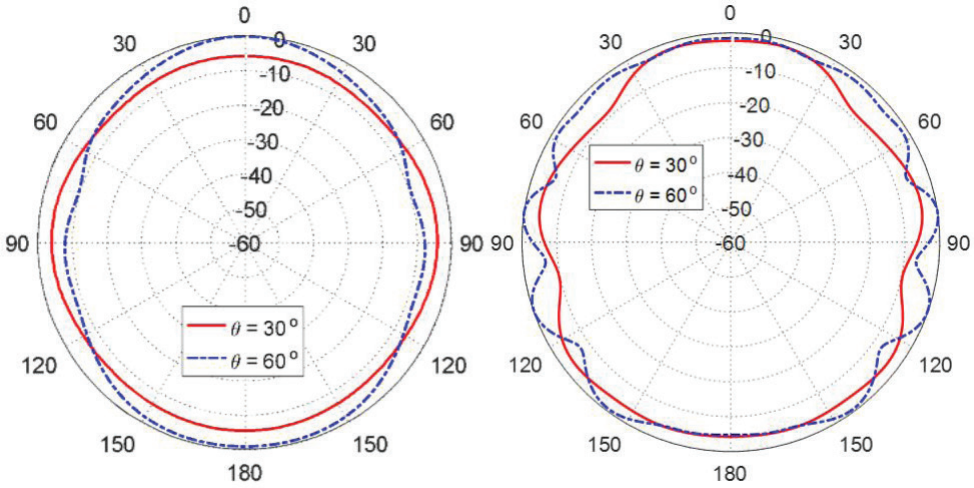

Fig. 7. Radiation patterns in the azimuth planes at 60 GHz for the dual-band microstrip patch antenna, (a) design "A" and (b) design "B".

3.2. Self and Mutual Coupling Coefficients for the Four-Port MIMO Antenna System

The dependence of the various self and mutual scattering parameters for the four-port MIMO antenna configuration, design "A", on the frequency is presented in Figure 8. It is shown that the self-scattering parameters representing the reflection coefficients at the antenna ports are almost identical over the entire frequency range and satisfy the impedance matching condition (low return loss) over the lower and upper frequency bands which are centered at 38 GHz and 60 GHz, respectively. The mutual scattering parameters show very weak coupling between the antennas' ports, where all these coefficients are maintained below -20 dB over the entire frequency range except for the coefficients $|S_{31}|$ and $|S_{42}|$ which exceed -20 dB at the resonant frequencies of the MIMO antennas. This is attributed to the relatively small horizontal separating distance between the antennas connected to ports (1) and (3) and that between the antennas connected to ports (2) and (4) as shown in Figure 2. However, for better performance regarding the coupling coefficients, the horizontal separation can be a little bit increased. Nevertheless, the effect of both the vertical and horizontal separations between the antennas significantly affects the coupling coefficients and such an effect is investigated later on.

On the other hand, for MIMO antenna system of design "B", the frequency response of the various self and mutual scattering parameters is presented in Figure 9. The self-scattering parameters at the antenna ports show impedance matching over the lower and upper frequency bands with better performance than that achieved by design "A". Also, the mutual scattering parameters show very weak coupling between the antennas' ports, where all these coefficients are maintained below -30 dB over the entire frequency band. Owing to the wider separation distances between the elements, the isolation between the antenna ports is significantly better than that achieved by the MIMO antenna system of design "A".

http://dx.doi.org/10.21622/ACE.2022.02.2.068

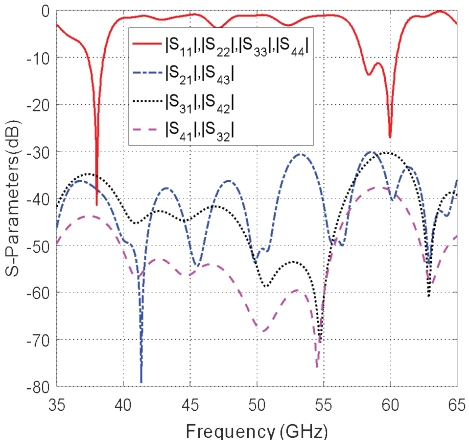

Fig. 8. Dependence of the self and mutual scattering parameters of the proposed four-port MIMO antenna system of design "A" on the frequency over a wide band.

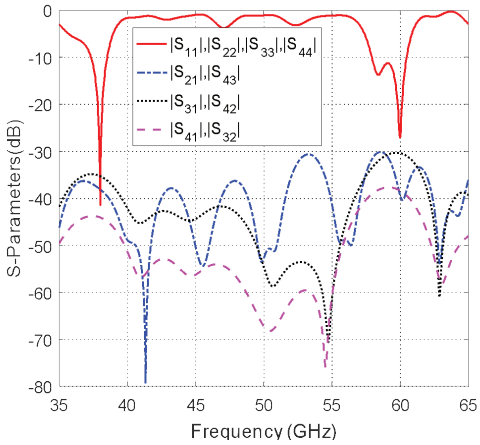

Fig. 9. Dependence of the self and mutual scattering parameters of the proposed four-port MIMO antenna system of design "B" on the frequency over a wide band.

3.3. Study of the Isolation between the Antenna Ports through the Surface Current Distribution

The mutual coupling between the antenna ports in a MIMO antenna system can be investigated by studying the surface current distribution on the patch antennas when a single port is excited alone. It is shown in Figure 10 that the surface current almost vanishes on the unexcited patches at 38 GHz. As shown in Figures 10(a) and 10(b), the surface current has a large value on the feedlines and on the patches attached to the (excited) ports "1" and "3", respectively and is almost zero elsewhere. This gives a strong indication to a high level of isolation between the antenna ports; that is there is almost no mutual current induced on the unexcited antenna elements. Figure 11 shows the current distribution on the excited patch surface (attached to port "1") at 38 GHz. As shown in this figure, the current is concentrated on the first patch and is negligible on the second patch showing the same behavior of a single antenna element radiating at 38 GHz.

At 60 GHz, the surface current distribution is presented in Figures 12(a) and 12(b) when each of the ports "1" and "3", respectively, is excited alone. One of the known coupling mechanisms of printed antennas is the surface waves propagating on the substrate-air interface. This can be seen in the area surrounding the excited patches where the (circular) wave fronts of the propagating surface waves are formed as concentric circular patterns of the surface current distribution on the top surface of the substrate. In comparison to Figures 10(a) and 10(b) for the surface waves generated at 38 GHz, the surface waves generated at 60 GHz seem to be stronger. This results in that the magnitude of the coupling coefficients $|S_{31}|$ and $|S_{42}|$ at 60 GHz is greater than its magnitude at 38 GHz as already shown in Figures 10 and 13 which show the current distribution on the excited patch surface (attached to port "1") at 60 GHz. As shown in Figure 13, the current is nearly equally distributed on the first and second patches showing the same behavior of a single antenna element operating at 60 GHz where the combined structure of the two patches is responsible for the radiation into the far zone.

It should be noted that when exciting each of the ports "2" and "4" alone, identical surface current distributions described for port "1" and "3" exist on the corresponding

http://dx.doi.org/10.21622/ACE.2022.02.2.068

patches and their surrounding areas on the substrate top surface at both 38 and 60 GHz.

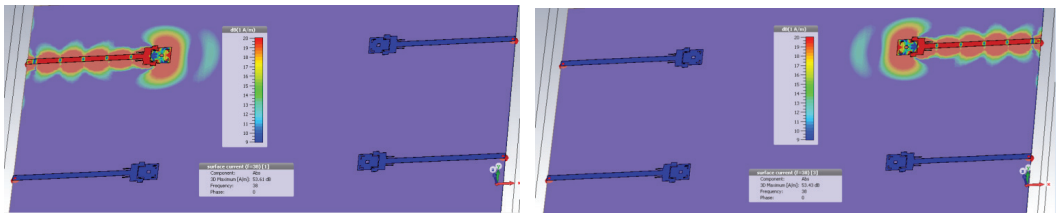

(a) (b)

Fig. 10. Surface current distribution on the four patches and the substrate when a single port is excited at 38 GHz, (a) port "1" is excited alone, (b) port "3" is excited alone.

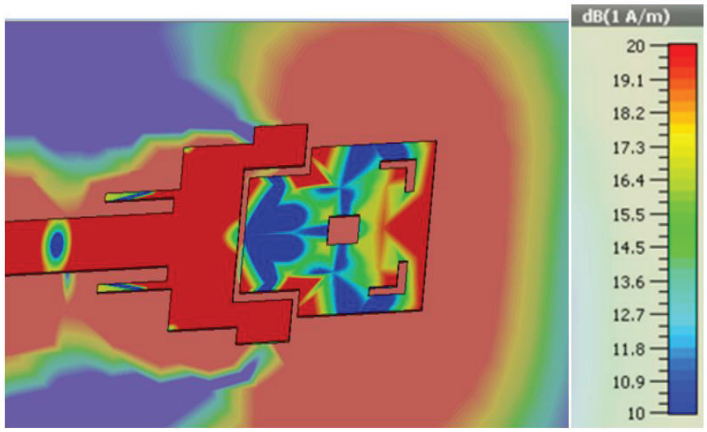

Fig. 11. Surface current distribution on the excited patch and the surrounding area of the substrate when a port "1" is excited alone at 38 GHz.

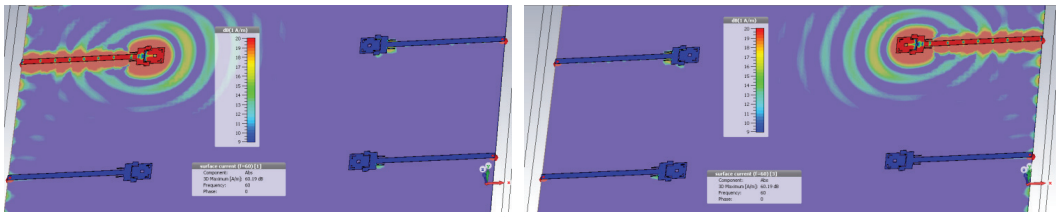

(a) (b)

Fig. 12. Surface current distribution on the four patches and the substrate when a single port is excited at 60 GHz, (a) port "1" is excited alone, (b) port "3" is excited alone.

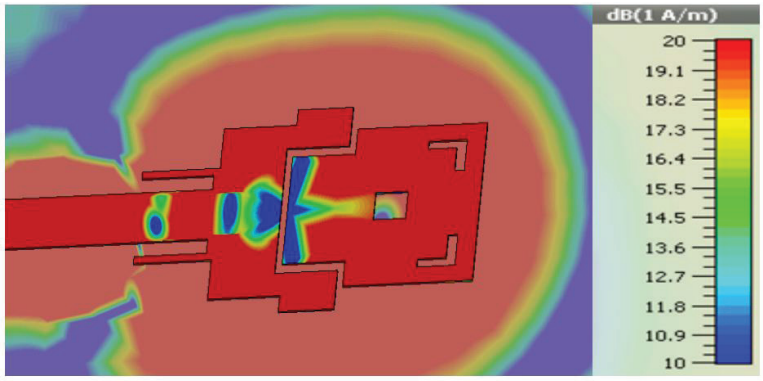

Fig. 13. Surface current distribution on the excited patch and the surrounding area of the substrate when port "1" is excited alone at 60 GHz 60 GHz.

http://dx.doi.org/10.21622/ACE.2022.02.2.068

3.4. Parametric Study of the Separation between the Patch Antennas on the Performance of the MIMO Antenna System

The horizontal and vertical separations D_H and D_V have major effects on the performance of the MIMO antenna system. Decreasing the separation between the adjacent antennas increases the mutual coupling between them, which, in turn has bad effects on the self-impedance of each element of the MIMO antenna system. Also, the ECC and the DG are badly affected by decreasing the separations between the antennas in a MIMO system. On the other hand, increasing the distances between the antennas may be limited by the physical dimensions of the supporting frame of the mobile handset itself. The following subsections are dedicated for presenting and discussing the possibility of increasing the separating distances between the elements of the proposed MIMO antenna system on the VSWR of the elements, the coupling coefficients between the different ports, the ECC and the DG of the MIMO system. Definitely, the horizontal separation, D_H, in both the proposed designs "A" and "B" has a greater effect on the MIMO system performance than the vertical separation, D_V as the direction of propagation of the substrate surface waves is horizontal as seen in the surface current distribution presented in Fig. 10 and Fig.12.

3.4.1. Effect of the separation between the patch antennas on the VSWR at the antenna ports

The effects of the horizontal separation on the VSWR at each of the four ports of the proposed MIMO system of design "B" are presented in Figure 14 at 38 and 60 GHz. As shown in the figure, the VSWR seems to be independent of the horizontal separation and each of the four antennas is perfectly matched even when the antennas are very close to each other. The VSWR calculated for a horizontal separation of 1 mm is almost equal to that calculated for a separation of 20 mm. This can be attributed to the design of the antenna with dual-patch structure that concentrates the fields beneath the first patch in a region far enough from the front edge of the second patch. Also, the weak mutual effects among the antennas is owed to the selected thin substrate which confines the fields in the dielectric region just below the radiating patches and, thereby, reduces the region into which the field is fringing preventing it from arriving to the other antennas. Moreover, this substrate is characterized by its very low loss due to its very small loss tangent (δ =0.001) which reduces the substrate currents. The surface waves generated in low-loss thin substrate at one antenna are too weak to arrive at the other antennas even when they are very close to each other.

3.4.2. Effect of the separation between the patch antennas on the coupling coefficients

The frequency responses of the mutual coupling coefficients between each pair of the four antennas of the MIMO system of design "A" are presented in Figures 15 (a) and 15(b) for different values of the horizontal and vertical separations, respectively. As shown in the figures, decreasing the horizontal separation has a worse effect on the coupling coefficients than the effect of decreasing the vertical separation. Increasing both the horizontal and vertical separations leads to global and monotonic decrease of the coupling coefficients, which in turn, enhances the MIMO antenna performance and increases the diversity gain. The drawback of increasing the separations between the printed patch antennas is the increase of the MIMO antenna size. It is shown that increasing the horizontal separation from 3.38 mm to 6.38 mm has the effect of decreasing the maximum coupling coefficient from about -18 dB to about -22.5 dB. To compromise between the MIMO antenna size and the performance regarding the mutual coupling between the four antennas, it

http://dx.doi.org/10.21622/ACE.2022.02.2.068

may be recommended to set the horizontal separation to 6.38 mm and to set the vertical separation to 2.46 mm for the MIMO system of design "A".

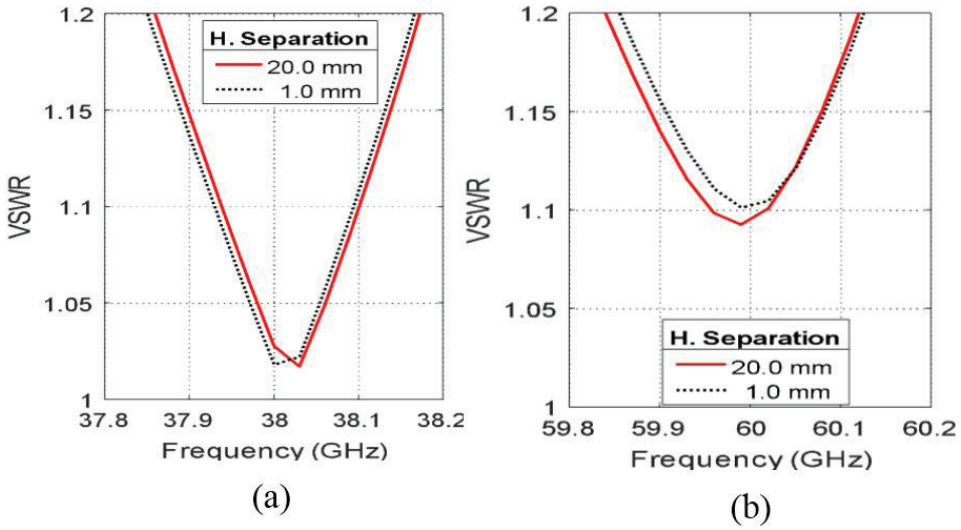

Fig. 14. Dependence of the VSWR on the frequency for all the four ports of the proposed MIMO system of design "B" for different values of the horizontal separation, D_H at (a) 38 GHz and (b) 60 GHz.

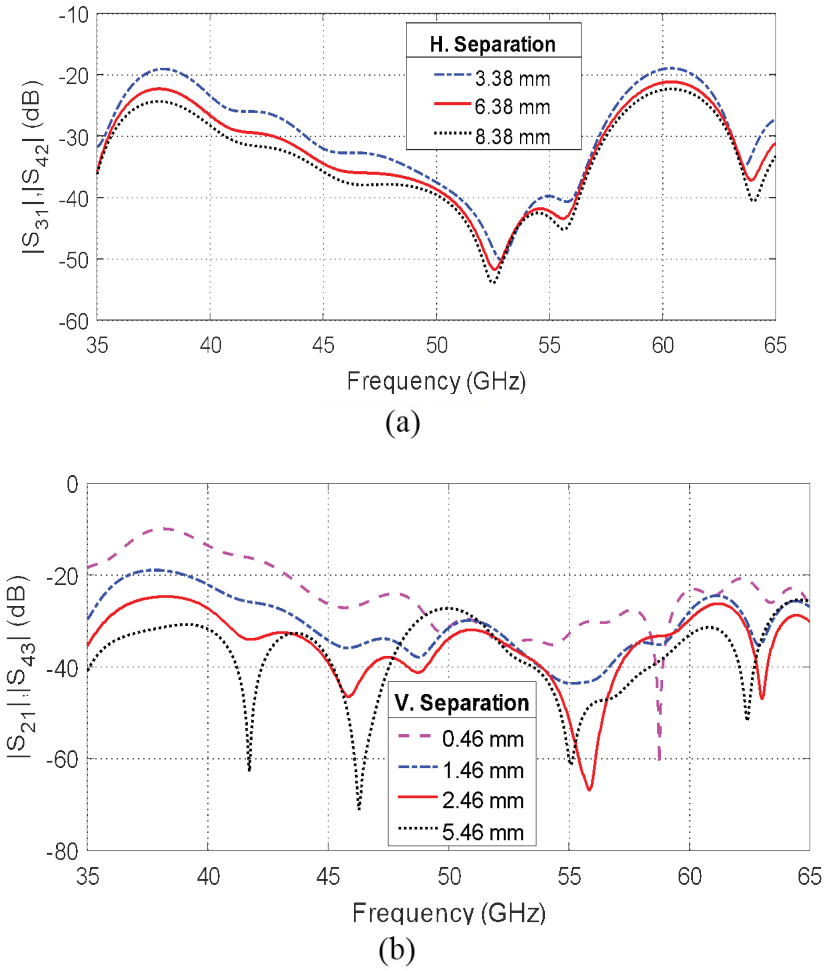

Fig. 15. Frequency dependence of the mutual coupling coefficients between the antenna elements of the four-port MIMO system of design "A" for different values of (a) horizontal separations, DH and (b) vertical separations between the patches, DV.

http://dx.doi.org/10.21622/ACE.2022.02.2.068

3.4.3. Effect of the separation between the patch antennas on the ECC and DG

The frequency responses of the ECC and the DG of the proposed four-port MIMO antenna system of the design "A" are presented in Figure 16 for different values of the horizontal separation between the antennas. As shown in the figure, increasing the separating distances between the antennas of the MIMO system improves the ECC and DG. Also, it is shown that at the center frequencies of the lower and upper bands of the antenna operation (38 and 60 GHz) and over the entire width of each band, the ECC is very low (almost 0) and, consequently, the DG is almost 10 for all the values of the horizontal separating distance between the antennas. This is considered to be the best achievable performance for a MIMO antenna system.

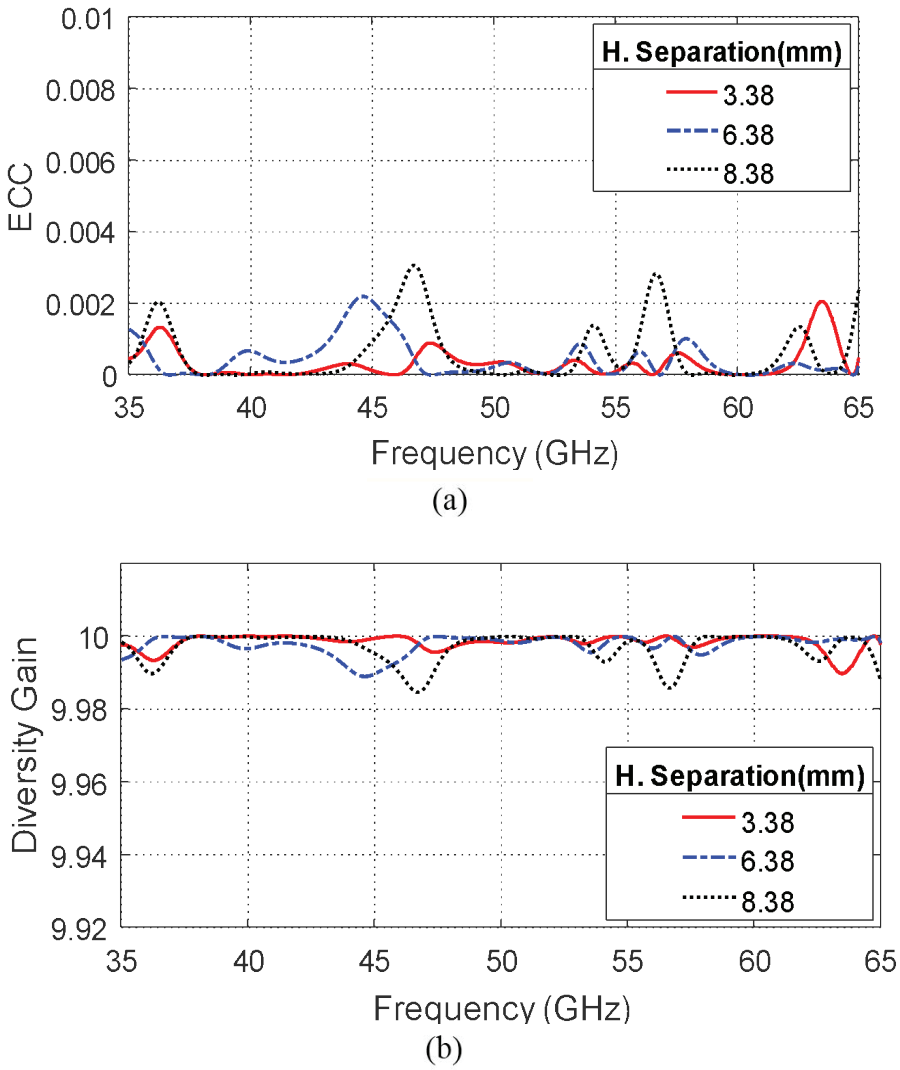

Fig. 16. Frequency dependence of the (a) ECC and (b) DG of the four-port MIMO antenna system of design "A" for different values of the horizontal separation distance between the patches.

3.5. Radiation Patterns of the MIMO Antenna System

The radiation patterns produced by the proposed MIMO antenna system of the design "A" when exciting each port alone at f=38 GHz and f=60 GHz are presented in Figures 17 and 18, respectively. It is shown that the produced radiation patterns are omnidirectional in the azimuth planes and have the balloon-like shape in the vertical

http://dx.doi.org/10.21622/ACE.2022.02.2.068

planes which are recommended for the 5G mobile phone MIMO antennas. It is also noticed that the radiation pattern produced when exciting each port alone is not badly affected by the other unexcited antennas. Besides the reasonable size of the overall MIMO antenna system and the fairly long distances between the antennas that produce high diversity gain, the radiation patterns provide excellent solution for an efficient operation as a 5G mobile phone antenna.

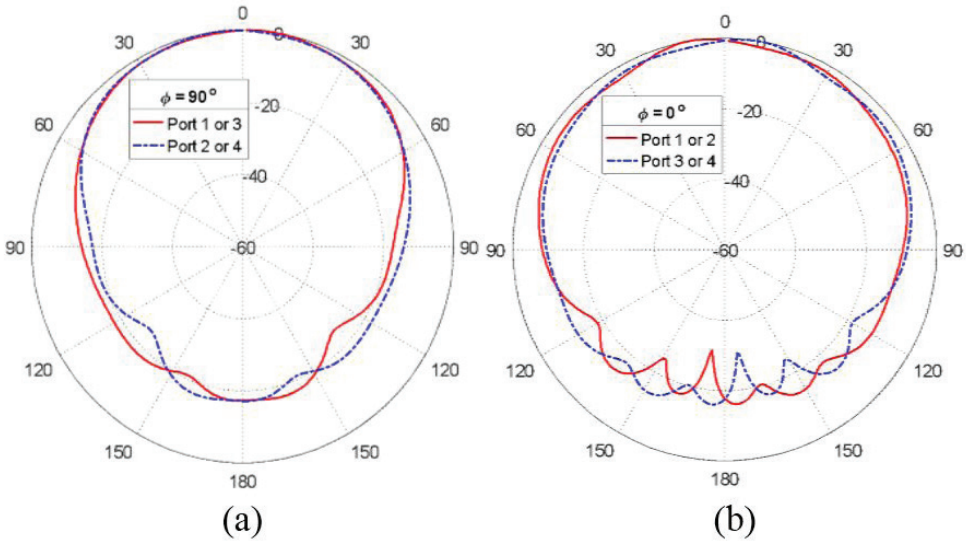

Fig. 17. Radiation patterns in the (a) H- and (b) E-planes for the proposed four-port MIMO antenna system of the design "A" using the dual-band microstrip patch proposed in the present work at f=38 GHz.

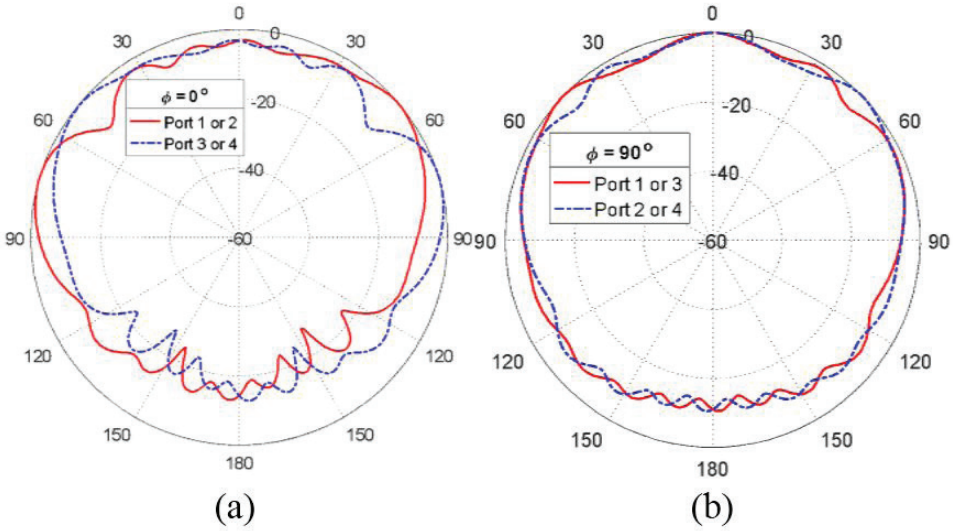

Fig. 18. Radiation patterns in the (a) E- and (b) H-planes for the proposed four-port MIMO antenna system of the design "A" using the dual-band microstrip patch proposed in the present work at f=60 GHz.

3.6. Efficiencies of the MIMO Antenna System

The radiation and total efficiencies of the proposed four-port MIMO antenna system of the design "B" when each port is excited alone are listed in Table 2. At both operating frequencies of the proposed MIMO antenna system, the radiation efficiency can be considered fairly high with respect to the relatively high values of the operating frequencies.

http://dx.doi.org/10.21622/ACE.2022.02.2.068

TABLE 2. Radiation and Total Efficiencies of the Proposed Four-port MIMO Antenna System of the Design "B".

Horizontal Separation	Efficiency	Frequency (GHz)	
		38	60
20.0 mm	Total	89.4%	78.1%
	Radiation	89.37%	77.8%
1.0 mm	Total	89.87%	79.0%
	Radiation	90.11%	79.5%

3.7. Envelope Correlation Coefficient and Diversity Gain

The dependencies of the ECC and the DG of the proposed four-port MIMO antenna system of the design "B" on the frequency are presented in Figure 19. It is shown that at the operating frequencies 38 and 60 GHz and over the entire width of the lower and upper bands, the ECC is very low (almost 0) and, consequently, the DG is very high (almost 10). This can be considered as the optimum performance of MIMO antenna system. It should be noted that the relative positions of the antennas in the pair (1, 2) are the same as those in the pair (3, 4); this leads to identical ECC and DG as shown in Figure 19. The same applies for the antenna pairs (1,3) and (2,4) and, also, for the antenna pairs (1,4) and (2,3).

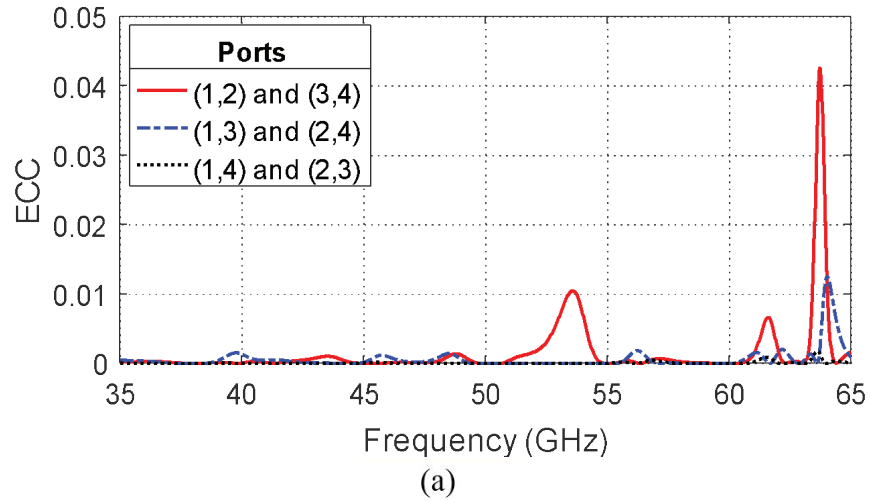

(a)

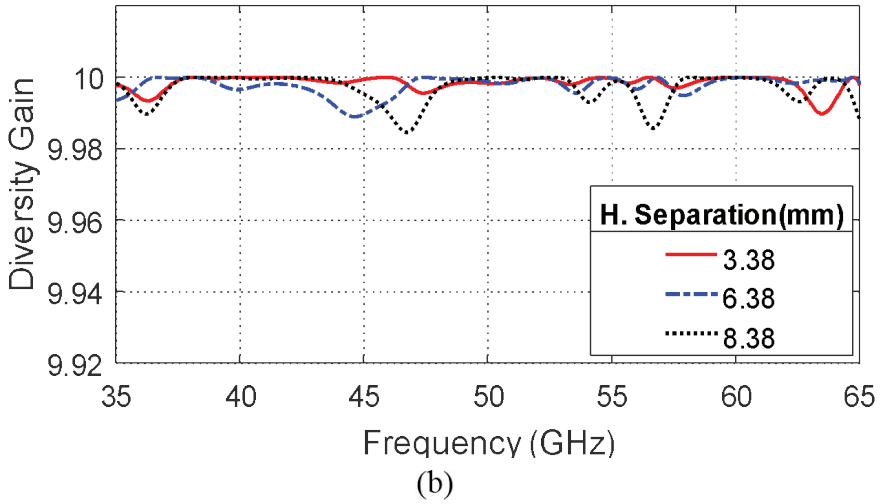

(b)

Fig. 19. Frequency dependence of the (a) ECC and (b) DG of the four-port MIMO antenna system of the design "B".

http://dx.doi.org/10.21622/ACE.2022.02.2.068

4. FABRICATION AND MEASUREMENTS OF THE MIMO ANTENNA SYSTEM PROTOTYPE

This section is concerned with the presentation of the experimental measurements of the four-port MIMO antenna system constructed by the dual-band microstrip patch antenna described above. Prototypes are fabricated for the four-port MIMO antenna system of the design "B". To confirm the accuracy of the assessed performance for the proposed MIMO antenna system, the measurement results are compared to those obtained by electromagnetic simulation using the commercially available CSTTM software package.

4.1. Measurements of the Return Loss at Each Port

The prototype shown in Figure 20(a) is fabricated for the purpose of experimental assessment of the performance of the proposed dual-band four-port MIMO antenna system. The vector network analyzer (VNA) Rhode and Schwartz model ZVA67 is used for measuring the frequency response of the reflection coefficients $|S_{11}|$ and $|S_{22}|$ at the ports "1" and "2" (the corresponding measurements for ports "3" and "4" are almost identical). Two 1.85 mm end-launch connectors from Southwest Microwave Incorporation are used for connecting the corresponding antennas to the VNA as shown in Figure 20(b).

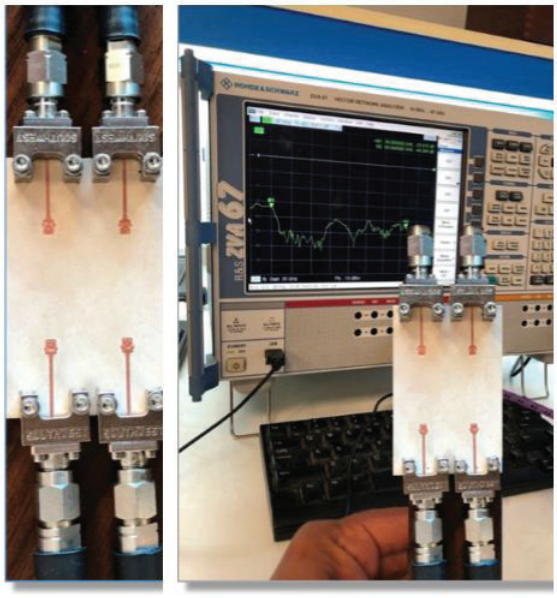

(a) (b)

Fig. 20. Measurement of the reflection coefficients $|S_{11}|$ and $|S_{22}|$ of the proposed four-port MIMO antenna system using the VNA Rhode and Schwartz model ZVA67. (a) Fabricated prototype, (b) Measurement of the S-parameters.

The frequency dependencies of $|S_{11}|$ and $|S_{22}|$ are presented in Figure 21 (relative to 50 Ω characteristic impedance of the microwave source) compared to the simulation results showing excellent agreement. The measured bandwidths over which |S11|< -10 dB $|S_{11}|$ <-10dB are shown to be wider than those obtained by simulation. The bandwidth measured at 38 GHz is about 2.0 GHz, whereas the bandwidth obtained by simulation is about 1.2 GHz. The measured bandwidth at 60 GHz is about 3.2 GHz, whereas the simulated one is about 2.52 GHz. It is shown that the width of upper frequency band obtained by measurements is centered at about 60 GHz, whereas the upper band obtained by simulation is shown to be shifted towards the left and centered at about 59 GHz. It is shown that the center frequency of the

http://dx.doi.org/10.21622/ACE.2022.02.2.068

lower band measured at port "2" is slightly shifted towards the right.

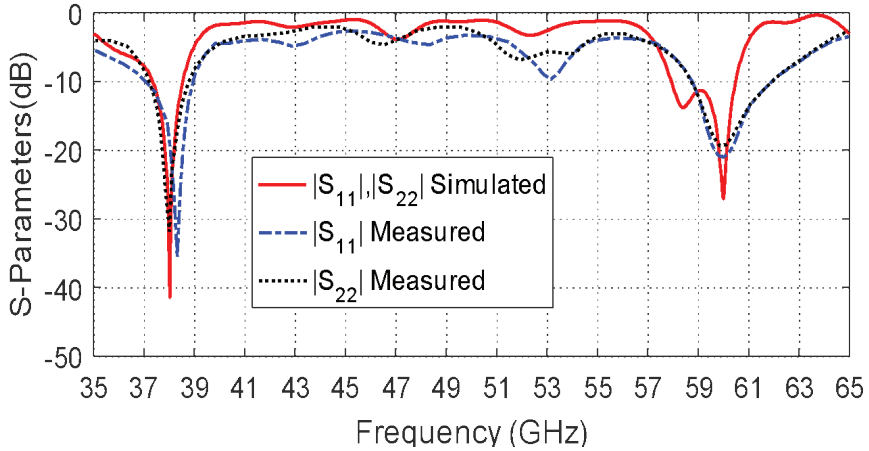

Fig. 21. Measured frequency responses of the reflection coefficients, $|S_{11}|$ and $|S_{22}|$, of the proposed dual-band four-port MIMO system.

4.2. Measurements of the Isolation between the Ports

The frequency responses of the transmission coefficient, $|S_{21}|$, of the proposed dual-band four-port MIMO antenna system of design "B", obtained by experimental measurements are presented in Figure 22 compared to those obtained by simulation. Both simulation and experimental results show very low values of the mutual coupling between the antennas connected to ports "1" and "2" over the entire frequency range. This indicates very high performance of such a MIMO antenna system regarding the ECC and DG.

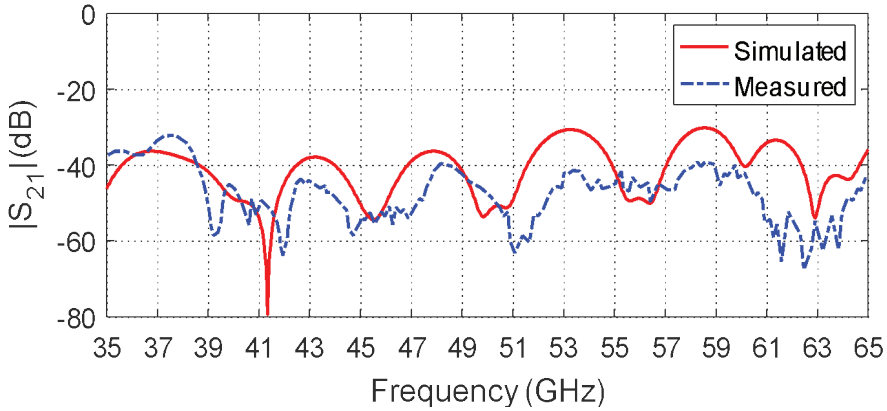

Fig. 22. Measured frequency response of the transmission coefficient, $|S_{21}|$, of the proposed dual-band four-port MIMO antenna system (relative to 50 Ω characteristic impedance of the microwave source) compared with the simulation results.

4.3. Measurements of the Radiation Patterns and Maximum Gain for Each Port

The experimental setup for measuring the radiation patterns and the maximum gain of the proposed four-port MIMO antenna system is presented in Figure 23. The VNA Rhode and Schwartz model ZVA67 operating in the two-port measurement mode is used for this purpose by measuring the transmission coefficient $|S_{21}|$ through the antenna under test and the reference-gain linearly-polarized horn antennas models LB-018400 (for 38 GHz band) and LB-12-10-A (for 60 GHz-band).

http://dx.doi.org/10.21622/ACE.2022.02.2.068

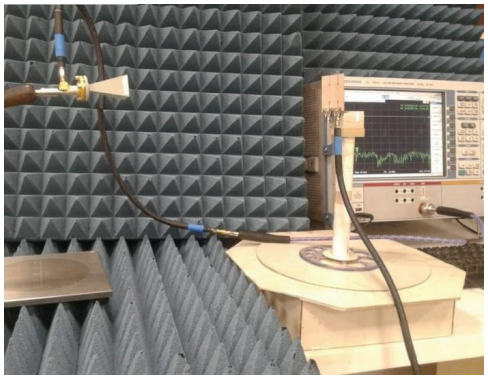

Fig. 23. Experimental setup for measuring the radiation pattern and gain while exciting each port of the MIMO antenna system alone.

The elevation radiation patterns measured in the planes ϕ =0° (E-plane) and ϕ=90° (H-plane) of the proposed four-port MIMO antenna system of design "B" are presented in Figures 24 and 25 at 38 GHz and 60 GHz, respectively. The measured and simulated radiation patterns show good agreement. The maximum gain values obtained by measurement are 6.1 dBi and 5.2 dBi at 38 GHz and 60 GHz, respectively, which agree with the measured values (6.5 dBi and 5.5 dBi at 38 GHz and 60 GHz, respectively).

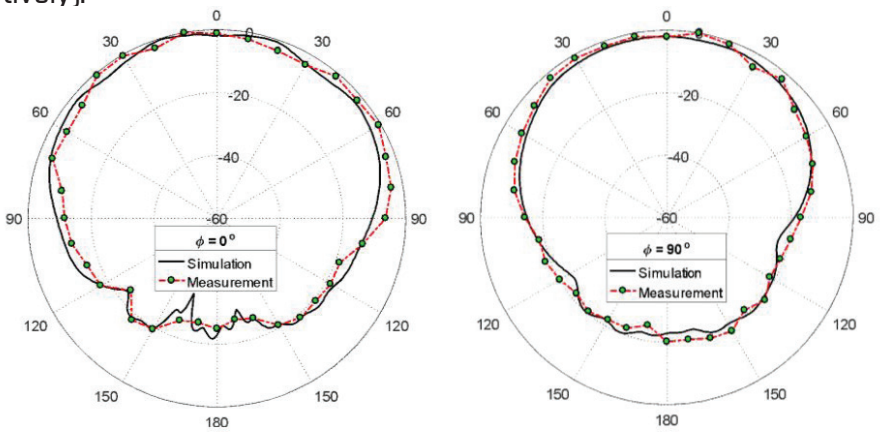

(a) E-plane ($\phi = 0°$) (b) H-plane ($\phi = 90°$)

Fig. 24. Measured radiation patterns at 38 GHz of the dual-band antenna compared with the simulation results while exciting each port of the MIMO antenna system of design "B".

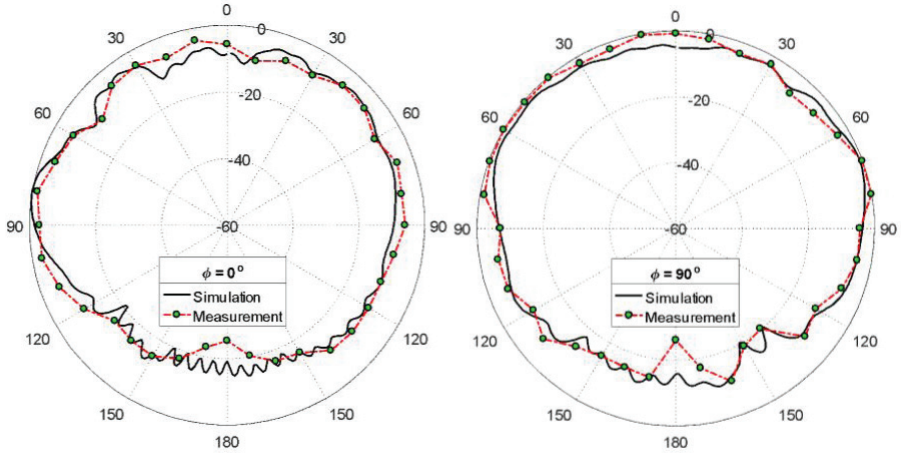

(a) E-plane ($\phi = 0°$) (b) H-plane ($\phi = 90°$)

Fig. 25. Measured radiation patterns at 60 GHz of the dual-band antenna compared with the simulation results while exciting each port of the proposed four-MIMO antenna system of design "B".

http://dx.doi.org/10.21622/ACE.2022.02.2.068

5. COMPARATIVE ASSESSMENT OF PERFORMANCE

In the frequency band centered at 38 GHz, the dependence of the reflection coefficient $|S_{11}|$ obtained for the MIMO antenna proposed in the present work on the frequency is compared to those presented in [23], [24] and [25] as shown in Figure 26. The corresponding values of the center frequencies, return loss and impedance matching bandwidth are specified in Table 3. It is shown that the present work outperforms other published work concerning the center frequency and corresponding return loss. The present impedance matching bandwidth is shown to be better than the work of [25] and is approximately the same as the work of [23] which has a higher value of the return loss compared to the present work.

In the frequency band centered at 38 GHz, the dependence of the coupling coefficient $|S_{21}|$ obtained for the MIMO antenna proposed in the present work on the frequency is compared to those presented in [17] and [28] as shown in Figure 27. The maximum value of the coupling coefficient achieved in the present work, [17] and [28] is stated in Table 4. This means that the ECC and consequently the DG achieved by the MIMO system proposed in the present work is superior to those introduced in the mentioned published results.

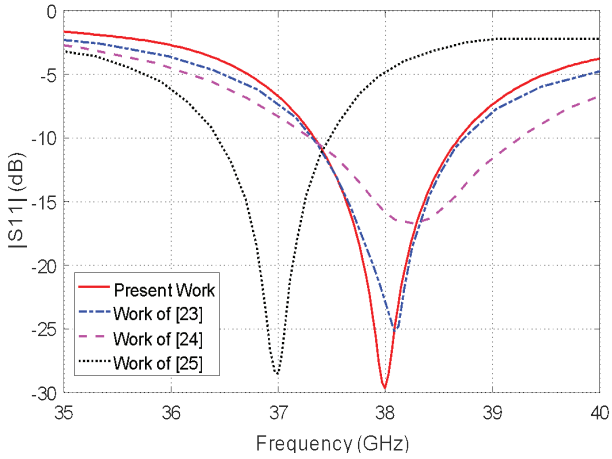

Fig. 26. Frequency response of the reflection coefficient, $|S_{11}|$, measured at port "1" of the MIMO antenna system proposed in the present work in the frequency band centered at 38 GHz in comparison to those presented in other publications.

TABLE 3. MIMO Antenna Performance at 38 GHz (Port 1)

Performance Measure	Work			
	[23]	[24]	[25]	Present
f_0 (GHz)	38.1	38.3	37.0	38.0
$\|S_{11}\|_{dB}$ (38 GHz)	-23	-15	-5	-30
BW (GHz)	1.4	2.0	1.0	1.4
Dimensions (mm)	55x110	6x6.25		50x30

In the frequency band centered at 60 GHz, the frequency response of the $|S_{11}|$ obtained for the antenna proposed in the present work through simulation is compared to those presented in [26] and [27] as shown in Figure 28. The minimum value of the return loss achieved in the present work, [26] and [27] is listed in Table 5. It is clear that the presented work surpasses the published work regarding the center frequency of the band of interest, return loss and impedance matching bandwidth. The bandwidth of the present work is about 4 times the work of [26] and has increased about 12 times the work of [27], which indicates a remarkable enhancement of the 60-GHz bandwidth.

http://dx.doi.org/10.21622/ACE.2022.02.2.068

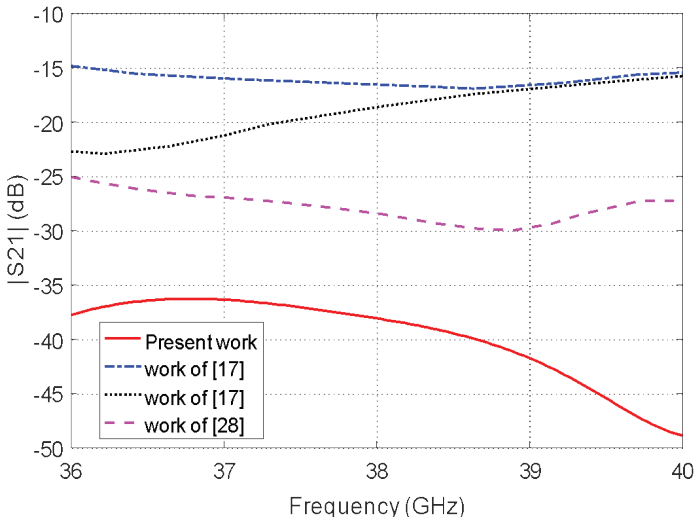

Fig. 27. Comparisons between the frequency responses of the coupling coefficients $|S_{21}|$ obtained in the present work for the proposed dual-band four-port MIMO antenna system in comparison to those obtained in [17] and [28] at 38 GHz.

TABLE 4. MIMO Antenna Performance at 38 GHz (Port 1 and 2)

Performance Measure	Work			
	[17]	[28]	[23]	Present
$\|S_{11}\|_{dB}$	-17	-12	-23	-28
$\|S_{22}\|_{dB}$	-15	-10	-23	-30
$\|S_{21}\|_{dB}$	-17	-28	-30	-38
ECC	1×10^{-7}	7×10^{-8}	1×10^{-10}	2×10^{-13}

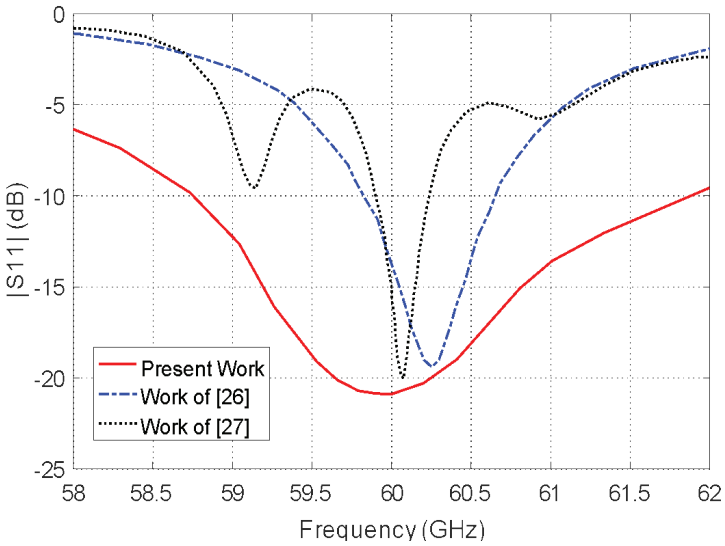

Fig. 28. Frequency response of the reflection coefficient, $|S_{11}|$, measured at port "1" of the MIMO antenna system proposed in the present work in the frequency band centered at 60 GHz in comparison to those presented in [26] and [27].

http://dx.doi.org/10.21622/ACE.2022.02.2.068

Table 5. MIMO Antenna Performance at 60 GHz (Port 1)

Performance Measure	Work		
	[26]	[27]	Present
f_0 (GHz)	60.26	60.10	60.00
$\|S_{11}\|_{dB}$ (60 GHz)	-14	-15	-21
BW (GHz)	1.5	0.5	6.3

6. CONCLUSION

A novel design is introduced for four-port MIMO antenna system for 5G mobile phones. The proposed MIMO antenna is constructed of microstrip patch antennas with novel compact design to operate in the 38/60 GHz dual-band. The single antenna is constructed as primary and secondary rectangular patches with some geometrical modifications to fulfil the required impedance matching and balloon-like radiation patterns for the lower and the upper frequency bands of operation. The first patch is fed in a direct way using a microstrip line with an inset feed and is mainly responsible for the lower band (38 GHz) radiation. On the other hand, the second patch is responsible for the upper frequency band (60 GHz) radiation and is fed through both capacitive and inductive coupling to the first patch. The performance of both the single-element antenna together with the four-port MIMO antenna system is assessed numerically and experimentally through investigations for both. It is shown that the results of the simulation agree with the results of the experimental measurements, and both show good performance for the single antenna as well as the MIMO antenna system. Although the dimensions of the antenna are slightly larger than those published in previous works of literature. However, the proposed MIMO antenna dimensions do not impede it from being used in 5G systems. The achieved bandwidths around 38 GHz and 60 GHz are about 2 GHz and 3.2 GHz, respectively. The minimum values for the return loss are -42 dB at 38 GHz and -47 dB at 60 GHz. The gain has a maximum value of about 6.5 dBi at 38 GHz, and about 5.5 dBi at 60 GHz. The mutual coupling coefficients are below -30 dB over the operational frequency bands. Also, it is shown that the envelope correlation coefficient (ECC) and the diversity gain (DG) for the four-port MIMO antenna system are suitable over the lower and upper frequency bands.

Author Contribution: Conceptualization: M.S., R.K, A.Z., and M.O.; methodology, M.S.; software, M.S.;
validation, M.S., formal analysis, M.S., M.O.; investigation, M.S.; resources, M.S., A.Z., R.K. and M.O.; data curation, M.S.; writing—original draft preparation, M.S.; writing—review and editing, A.Z., R.K. and M.O.; visualization, M.S.; supervision, A.Z., R.K, and M.O.; project administration, M.S.

Funding: This research has no external funding.

Conflicts of Interest: The authors declare no conflict of interest.

http://dx.doi.org/10.21622/ACE.2022.02.2.068

REFERENCES

[1] G. Das, A. Sharma, R. K. Gangwar, and M. S. Sharawi, "Performance improvement of multiband MIMO dielectric resonator antenna system with a partially reflecting surface," IEEE Antennas Wirel Propag Lett, vol. 18, no. 10, 2019, doi: 10.1109/LAWP.2019.2938004.

[2] S. Muhammad, A. S. Yaro, I. Ya'u, and A. T. Salawudeen, "Design of 5G Mobile Millimeter Wave Antenna," ATBU Journal of Science, Technology and Education, vol. 7, no. 2, 2019.

[3] N. O. Parchin et al., "Mobile-phone antenna array with diamond-ring slot elements for 5G massive MIMO systems," Electronics (Switzerland), vol. 8, no. 5, 2019, doi: 10.3390/electronics8050521.

[4] S. N. H. Sa'Don et al., "Analysis of graphene antenna properties for 5G applications," Sensors (Switzerland), vol. 19, no. 22, 2019, doi: 10.3390/s19224835.

[5] M. Ikram, N. Nguyen-Trong, and A. Abbosh, "Multiband MIMO microwave and millimeter antenna system employing dual-function tapered slot structure," IEEE Trans Antennas Propag, vol. 67, no. 8, 2019, doi: 10.1109/TAP.2019.2922547.

[6] M. Abirami, "A review of patch antenna design for 5G," in Proceedings - 2017 IEEE International Conference on Electrical, Instrumentation and Communication Engineering, ICEICE 2017, 2017, vol. 2017-December. doi: 10.1109/ICEICE.2017.8191842.

[7] P. A. Dzagbletey and Y. B. Jung, "Stacked microstrip linear array for millimeter-wave 5G baseband communication," IEEE Antennas Wirel Propag Lett, vol. 17, no. 5, 2018, doi: 10.1109/LAWP.2018.2816258.

[8] A. Rachakonda, P. Bang, and J. Mudiganti, "A compact dual band MIMO PIFA for 5G applications," in IOP Conference Series: Materials Science and Engineering, 2017, vol. 263, no. 5. doi: 10.1088/1757-899X/263/5/052034.

[9] O. M. Haraz, "Broadband and 28/38-GHz Dual-Band Printed Monopole/Elliptical Slot Ring Antennas for the Future 5G Cellular Communications," Journal of Infrared, Millimeter, and Terahertz Waves, vol. 37, no. 4. 2016. doi: 10.1007/s10762-016-0252-2.

[10] J. Saini and S. K. Agarwal, "Design a single band microstrip patch antenna at 60 GHz millimeter wave for 5G application," in 2017 International Conference on Computer, Communications and Electronics, COMPTELIX 2017, 2017. doi: 10.1109/COMPTELIX.2017.8003969.

[11] C. Şeker and M. Tahir Güneşer, "A Single Band Antenna Design for Future Millimeter Wave Wireless Communication at 38 GHz," European Journal of Engineering and Formal Sciences, vol. 2, no. 2, 2019, doi: 10.2478/ejef-2018-0009.

[12] Y. Li, C. Y. D. Sim, Y. Luo, and G. Yang, "Multiband 10-Antenna Array for Sub-6 GHz MIMO Applications in 5-G Smartphones," IEEE Access, vol. 6, 2018, doi: 10.1109/ACCESS.2018.2838337.

http://dx.doi.org/10.21622/ACE.2022.02.2.068

[13] N. O. Parchin et al., "Eight-Element Dual-Polarized MIMO Slot Antenna System for 5G Smartphone Applications," IEEE Access, vol. 7, 2019, doi: 10.1109/ACCESS.2019.2893112.

[14] R. Saleem, M. Bilal, H. T. Chattha, S. Ur Rehman, A. Mushtaq, and M. F. Shafique, "An FSS Based Multiband MIMO System Incorporating 3D Antennas for WLAN/WiMAX/5G Cellular and 5G Wi-Fi Applications," IEEE Access, vol. 7, 2019, doi: 10.1109/ACCESS.2019.2945810.

[15] X. S. Luo, Z. bin Weng, W. J. Zhang, and L. Yang, "Compact planar multiband MIMO antenna based on composite right/left-handed transmission line for mobile phone applications," Microw Opt Technol Lett, vol. 60, no. 6, 2018, doi: 10.1002/mop.31185.

[16] A. A. R. Saad and H. A. Mohamed, "Printed millimeter-wave MIMO-based slot antenna arrays for 5G networks," AEU - International Journal of Electronics and Communications, vol. 99, 2019, doi: 10.1016/j.aeue.2018.11.029.

[17] U. Rafique, H. Khalil, and Saif-Ur-Rehman, "Dual-band microstrip patch antenna array for 5G mobile communications," in Progress in Electromagnetics Research Symposium, 2017, vol. 2017-November. doi: 10.1109/PIERS-FALL.2017.8293110.

[18] C. Chu, J. Zhu, S. Liao, A. Zhu, and Q. Xue, "28/38 GHz Dual-band Dual-polarized Highly Isolated Antenna for 5G Phased Array Applications," in 2019 IEEE MTT-S International Wireless Symposium, IWS 2019 - Proceedings, 2019. doi: 10.1109/IEEE-IWS.2019.8804009.

[19] E. al Abbas, M. Ikram, A. T. Mobashsher, and A. Abbosh, "MIMO Antenna System for Multi-Band Millimeter-Wave 5G and Wideband 4G Mobile Communications," IEEE Access, vol. 7, 2019, doi: 10.1109/ACCESS.2019.2958897.

[20] Y. Hong and J. Choi, "60-GHz Array Antenna for mm-Wave 5G Wearable Applications," in 2018 IEEE Antennas and Propagation Society International Symposium and USNC/URSI National Radio Science Meeting, APSURSI 2018 - Proceedings, 2018. doi: 10.1109/APUSNCURSINRSM.2018.8608603.

[21] X. Tan, W. Wang, Y. Wu, Y. Liu, and A. A. Kishk, "Enhancing Isolation in Dual-Band Meander-Line Multiple Antenna by Employing Split EBG Structure," IEEE Trans Antennas Propag, vol. 67, no. 4, 2019, doi: 10.1109/TAP.2019.2897489.

[22] M. H. Sharaf, A. I. Zaki, R. K. Hamad, and M. M. M. Oma, "A novel dual-band (38/60 ghz) patch antenna for 5g mobile handsets," Sensors (Switzerland), vol. 20, no. 9, 2020, doi: 10.3390/s20092541.

[23] H. M. Marzouk, M. I. Ahmed, and A. A. Shaalan, "Novel dual-band 28/38 GHz MIMO antennas for 5g mobile applications," Progress In Electromagnetics Research C, vol. 93, 2019, doi: 10.2528/PIERC19032303.

[24] D. Imran et al., "Millimeter wave microstrip patch antenna for 5G mobile communication," in 2018 International Conference on Engineering and Emerging Technologies, ICEET 2018, 2018, vol. 2018-January. doi: 10.1109/ICEET1.2018.8338623.

http://dx.doi.org/10.21622/ACE.2022.02.2.068

[25] J. Khan, D. A. Sehrai, and U. Ali, "Design of Dual Band 5G Antenna Array with SAR Analysis for Future Mobile Handsets," Journal of Electrical Engineering and Technology, vol. 14, no. 2, 2019, doi: 10.1007/s42835-018-00059-9.

[26] P. Cabrol and P. Pietraski, "60 GHz patch antenna array on low cost Liquid-Crystal Polymer (LCP) substrate," in 2014 IEEE Long Island Systems, Applications and Technology Conference, LISAT 2014, 2014. doi: 10.1109/LISAT.2014.6845230.

[27] G. Zhang, S. Pu, X. Xu, Y. Liu, and C. Wang, "Design of 60-GHz microstrip antenna array composed through circular contour feeding line," in 2016 Asia-Pacific International Symposium on Electromagnetic Compatibility, APEMC 2016, 2016. doi: 10.1109/APEMC.2016.7522931.

[28] Y. W. Hsu, T. C. Huang, H. S. Lin, and Y. C. Lin, "Dual-Polarized Quasi Yagi-Uda Antennas with Endfire Radiation for Millimeter-Wave MIMO Terminals," IEEE Trans Antennas Propag, vol. 65, no. 12, 2017, doi: 10.1109/TAP.2017.2734238.